CRYSTAL GROWTH & DESIGN

Communication

pubs.acs.org/crystal

Growth of Large Hematin Crystals in Biomimetic Solutions

Katy N. Olafson,[†] Jeffrey D. Rimer,*[,†] and Peter G. Vekilov*[,†,‡]

[†]Department of Chemical and Biomolecular Engineering, and [‡]Department of Chemistry, University of Houston, Houston, Texas 77204, United States

ABSTRACT: Hematin crystallization is an essential component of the physiology of malaria parasites. Several antimalarial drugs are believed to inhibit crystallization and expose the parasites to toxic soluble hematin. Hence, understanding the mechanisms of hematin crystal growth and inhibition is crucial for the design of new drugs. A major obstacle to microscopic, spectroscopic, and crystallographic studies of hematin crystallization has been the unavailability of large hematin crystals grown under conditions representative of the parasite anatomy. We have developed a biomimetic method to reproducibly grow large hematin crystals reaching 50 μm in length. We imitate the digestive vacuole of *Plasmodium falciparum* and employ a two-phase solution of octanol and citric buffer. The nucleation of seeds is enhanced at the interface between the aqueous and organic phases, where an ordered layer of octanol molecules is known to serve as substrate for nucleation. The seeds are transferred to hematin-saturated octanol in contact with citric buffer. We show that the crystals grow in the octanol layer, while the buffer supplies hydrogen ions needed for bonds that link the hematin molecules in the crystal. The availability of large hematin crystals opens new avenues for studies of hematin detoxification of malaria parasites in host erythrocytes.

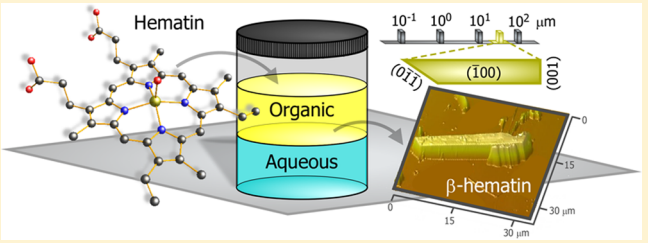

Malaria claims over one million lives annually and places up to 40% of the world population at risk, mostly throughout the equatorial regions of Africa, Oceania, South America, and Asia.[1,2] Alarmingly, the mortality caused by the disease has significantly increased since the 1960s due to evolution of strains of *Plasmodium* parasites resistant to drug combination treatments and their spread.[3] Delayed parasite clearance has been recorded even for the most recent artemisinin-based therapies.[4] The impending failure of the common antimalarial drugs underscores the need for research into the main processes of malaria pathophysiology.

The process of hematin crystallization is a pivotal point in understanding the mechanism(s) of action of the major quinoline antimalarial drugs.[5,6] The malaria parasites undergo multiple life cycle stages within the human host. The second stage occurs in the human erythrocytes, where free heme is released[7] as a byproduct of hemoglobin catabolism.[8,9] The heme, Fe(II)-protoporphyrin IX, is oxidized to hematin, Fe(III)-protoporphyrin IX (Fe(III) PPIX), which is toxic to the parasite at elevated concentrations. Free hematin concentrations are minimized by the formation of benign crystals, referred to as hemozoin.[10] The hemozoin crystals have approximate dimensions of 100 × 100 × (300−500) nm^3 and are located within the parasites' digestive vacuoles.[11]

Powder X-ray diffraction (XRD) from hemozoin extracted from *Plasmodium falciparum* and synthetic β-hematin crystals have demonstrated that the two materials are structurally identical triclinic crystals with space group $P\bar{1}$.[12−15] They are built of hydrogen-bonded head-to-tail dimers,[11] in which the central iron atom within the porphyrin ring of one hematin coordinates with a carboxylate oxygen of a second hematin.[12,13]

The parasite's digestive vacuole is biphasic, comprising lipid nanospheres suspended in an aqueous solution with pH in the range 4.8−5.5.[16,17] The lipids are remnants of endocytosis used to transport hemoglobin into the digestive vacuole and exhibit sizes up to several hundred nanometers.[18] Recent evidence suggests that hemozoin nucleates on a lipid film adsorbed to the digestive vacuole membrane.[19−21] The direction of crystal growth after nucleation, into an aqueous or lipid environment, has not been unambiguously identified.[21−25]

The traditional Western treatment for malaria, quinine, and its synthetic homologues, chloroquine, mefloquine, and others,[26−29] putatively work by blocking hematin addition to growing surfaces of hemozoin.[30] The sequestration of heme into hemozoin is a suitable target for new antimalarials and has been referred to as the "Achilles heel of the parasite". Thus, understanding the mechanisms of hematin crystallization and its inhibition by antimalarials is crucial for the development of new drugs that may overcome parasite resistance.[31]

Large β-hematin crystals that can be grown by the method presented herein represent a platform by which to study antimalarial drug action. These crystals are required to determine the relevant crystal properties and monitor the kinetics of crystal formation. Crystals with micrometer dimensions afford the application of optical, atomic force, and scanning electron microscopies; surface methods, such as grazing incidence X-ray and neutron diffraction;[32] and small/wide-angle X-ray scattering. Large crystal dimensions are

Received: February 23, 2014
Revised: April 7, 2014
Published: April 7, 2014

   dx.doi.org/10.1021/cg5002682 | *Cryst. Growth Des.* 2014, 14, 2123−2127

necessary for single-crystal X-ray crystallography, which could yield a more accurate molecular structure of β-hematin (relative to currently available powder diffraction data).[14,33] In turn, such structure would allow high-fidelity modeling of hematin−drug interactions and hematin aggregation. Moreover, large crystals would provide data on growth kinetics and inhibition rates by using high-sensitivity diagnostic techniques.[34−37] Lastly, β-hematin crystals are of interest due to their magnetic properties (the magnetic moment of the aqueous dimer of H_2O/HO-Fe(III)PPIX is μ = 4.21)[38,39] and could be potentially used as indicators in high throughput assays. Recently, crystals as large as 150 μm of a hematin−DMSO solvate were grown from a hematin solution in DMSO.[40] The nonphysiological synthesis and composition of these crystals constrain the physiological relevance and utility of the insights that they provide.

In this communication, we present a biomimetic approach to grow large β-hematin crystals. We model the environment in the parasites' digestive vacuole with a two-phase crystallization solution. To mimic the lipid bodies[27] of the parasites' digestive vacuole, we use 1-octanol, which has limited solubility in water. Since the lipid bodies are suspended in an aqueous medium, we assume that the lipid is saturated with water[41] and used water-saturated octanol,[42] referred to herein as wet octanol, as a model. Recent molecular dynamics simulations have elucidated the exchange of water molecules between the aqueous and octanol phases and shown the presence of an ordered layer of octanol at the interface;[43] this layer can serve as a nucleation template, analogously to the ordered lipids in the parasite's digestive vacuole.[19−21] To characterize the wet octanol, we employed dynamic light scattering with an ALV-5000/EPP device with laser wavelength λ = 628 nm, as discussed in Ketchum et al.[42] To maintain water content in octanol at saturation during data collection, we deposited about 100 μL of water at the bottom of the light scattering cuvette. The correlation and distribution functions of the scatted light in Figure 1A reveal that the wet octanol is not homogeneous but contains large scatterers that diffuse with a characteristic time τ = 11 ms. For the analyses of the DLS data, we used that the scattering vector $q = 4\pi n/\lambda \sin(\theta/2) = 2.01 \times 10^7$ m^{-1} at a scattering angle θ = 90°. We assumed a viscosity $\eta = 7.363 \times 10^{-3}$ Pa s and refractive index n = 1.429, equal to those of dry octanol. The radius R of the large scatterers was determined using the Stokes−Einstein relation

$$R = \frac{k_B T q^2}{6\pi\eta}\tau \qquad (1)$$

where k_B is the Boltzmann constant, T is the absolute temperature, and the diffusivity D was substituted with the term $D = (q^2\tau)^{-1}$. We obtain $R \cong 120$ nm. A similar characterization of dry octanol revealed no inhomogeneity. Thus, we conclude that the large scatterers reflected in the correlation function in Figure 1B are water droplets.

The presence of water droplets in the crystallization medium could have significant consequences for the nucleation and growth of β-hematin crystals. Thus, we tested the existence of water droplets in octanol with water content lower than the saturation limit and in water-saturated octanol in the presence of dissolved hematin. In both cases, the shoulder in the correlation function observed at long times in Figure 1A disappeared, indicating homogeneous solutions. The destabilization of the water droplets in the presence of hematin is counterintuitive: hematin is an amphiphilic molecule expected to lower the surface tension of the octanol−water interface and thus would be expected to stabilize the aqueous droplets. Our finding of opposite behavior suggests that hematin increases the solubility of water in octanol.

Dynamic light scattering (DLS) correlation functions similar to those in Figure 1A were recorded with 1-octanol held in contact with 25 mM aqueous citric buffer with pH 4.8. We conclude that buffer droplets of radius about 120 nm are present in citric buffer saturated octanol. The addition of hematin or the dilution with dry octanol leads to the disappearance of the DLS signal of the water droplets indicating that, similar to water-saturated octanol, the solution is homogeneous.

We tested if the commercial hematin, as received from Sigma-Aldrich, St. Louis, could provide seeds for the growth of large crystals. We characterized this reagent by powder XRD. The respective XRD pattern in Figure 1B does not possess any sharp peaks corresponding to Bragg reflections typical of β-hematin crystals.[22] We conclude that the commercial material is amorphous and cannot be directly used as a source of crystal seeds.

To produce crystal seeds, we used a thoroughly cleaned glass vial with an internal diameter 50 mm, in which we deposited wet octanol on top of citric buffer at pH of 4.8, as illustrated in Figure 2A. The octanol phase mimics the lipid nanospheres, while the citric buffer imitates the acidic environment of the parasite's digestive vacuole.[17] As expected, a well-defined interface exists between the two largely immiscible phases.

We prepared hematin solutions by dissolving commercial reagent at 2 mM in a 0.1 M NaOH (aq), following published procedures.[27,42] To minimize hematin oxidation, we limited the exposure of this solution to air to less than 30 min.[44] After all particulate matter dissolved, we filtered 0.5 mL of the hematin solution through a 0.22 μm filter. Using a syringe, we divided this aliquot into ca. 20 droplets and deposited them at the octanol/citric buffer interface, as illustrated in Figure 2A. Brown clusters formed at the interface within approximately 10 min after hematin addition. We incubated the two-phase solution at 23 °C for 12−14 days with minimal exposure to light. During the incubation, the pH of the citric buffer layer shifted to

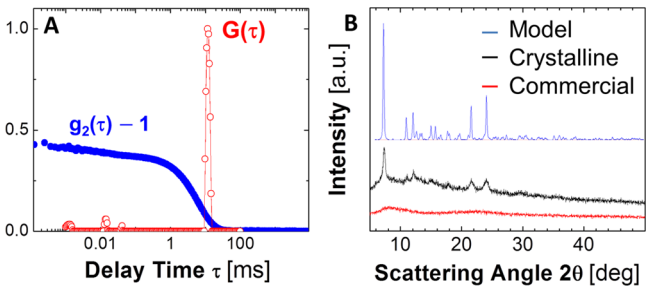

Figure 1. Characterization of the water-saturated octanol solvent and the commercial hematin preparation. (A) Correlation function $g_2(\tau)$ and intensity distribution function $G(\tau)$ obtained by dynamic light scattering from wet octanol. The data reveal the presence of a relatively monodisperse species of radius ca. 120 nm, which are likely water droplets. (B) Powder X-ray diffraction patterns of hematin: top, a model pattern computed using the package Diamond and hematin structure coordinates from the Cambridge Structural Database; middle, crystals grown in the laboratory following published procedures;[46] and bottom, porcine hematin as received from Sigma-Aldrich, indicating that the commercial material is predominately amorphous.

dx.doi.org/10.1021/cg5002682 | Cryst. Growth Des. 2014, 14, 2123−2127

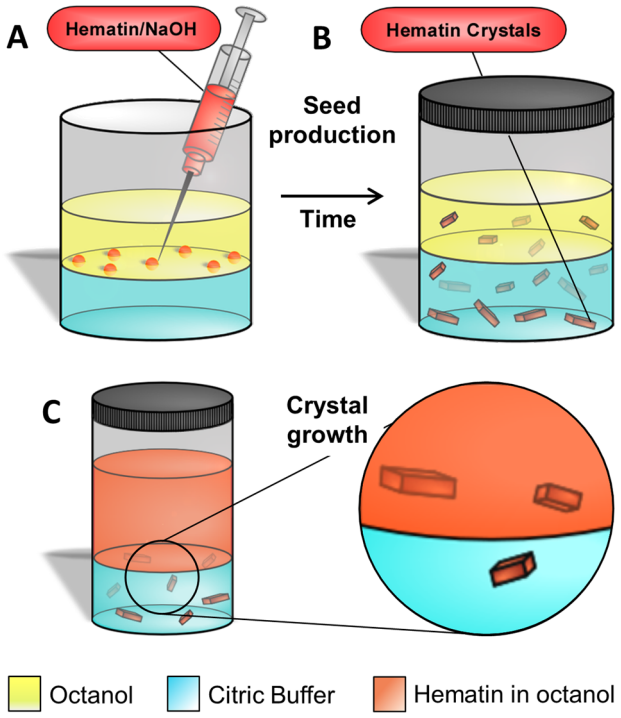

Figure 2. Illustration of the biomimetic experimental procedure. (A, B) Production of seed crystals. (A) In a glass vial with diameter 50 mm, we placed octanol on top of citric buffer at pH 4.80. Holding the two-phase solution at 37 °C, we deposited several droplets with a total volume 0.5 mL of a 2 mM hematin solution in 0.1 M NaOH at the octanol–buffer interface. (B) We incubated this solution at 23 °C for 12–14 days. Every 4–6 days, including immediately before crystal extraction, we sonicated the solution for 2 min at 25 °C. (C) We removed 50 or 100 mL of the citric buffer layer, in which the seeds are suspended, and deposited it into 200 mL of water-saturated octanol, in which hematin is dissolved at concentrations between 0.1–0.4 mM, exceeding the solubility of 0.07 mM. We incubated this solution for 2–4 days at 23 °C. The crystals likely grow in the octanol phase; some of them sediment the citric buffer under the influence of gravity as illustrated in the callout.

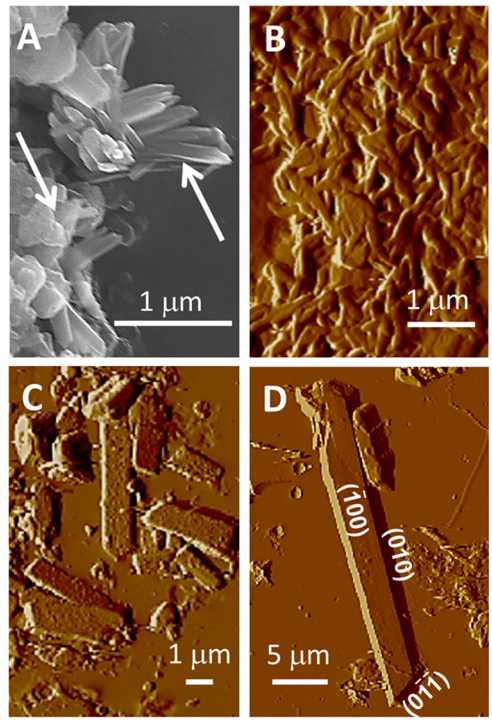

Figure 3. Crystal size and morphology at different stages of the growth procedure. (A) An SEM image revealing crystalline (indicated with an upward arrow) and apparently amorphous (indicated with a downward arrow) material isolated from the seed-preparation solution after about 30 min of growth. The crystals are about 600 nm long. (B) Deflection AFM image of microcrystals isolated after 1.5 h of growth reveals a higher yield of faceted microcrystals and fewer amorphous aggregates; the crystal size is the same as in A. (C) Deflection AFM image of 3–5 μm crystals isolated from the hematin-saturated two-phase solution after about 1 h after seeding. (D) A well-faceted 28 μm long crystal grown in the hematin saturated two-phase solution for 16 days.

slightly higher pH values due to neutralization by the added NaOH but always remained below 5.1. We sonicated this solution for approximately 2 min prior to removing aliquots for time-elapsed studies. Scanning electron microscopy (SEM) and atomic force microscopy (AFM) images in Figure 3A,B reveal that 30 min after hematin deposition the solution contains a mixture of faceted elongated formations, likely crystals, of size about 600 nm and what appear to be amorphous clusters. As time progresses, the quantity of amorphous material decreases, and the average crystal size increases. The phase transformation of hematin from amorphous solid to crystalline material is expected since the former is more soluble than the latter. SEM and AFM revealed that after 2 weeks, the crystals were approximately 2 μm in length. While these microcrystals were found in the aqueous phase, it is possible that they sediment from the organic phase. Hence, we cannot judge from these observations the location of their nucleation and growth. The process of formation of microcrystals is schematically depicted in Figure 2B.

Extended incubation of the two-phase crystallization solution illustrated in Figure 2B for up to 4 weeks did not yield crystals larger than 2–3 μm, likely due to depletion of soluble hematin. The deposition of greater volumes of hematin dissolved in 0.1 M NaOH failed to increase the crystal size, likely due to the documented pH increase in the citric buffer layer. Higher pH increases hematin solubility in the aqueous phase and reduces its concentration in the octanol phase; both consequences may induce growth cessation. Increasing the concentration of hematin in the initial NaOH solution led to smaller crystals likely due to the resulting higher numbers of nucleated crystals and corresponding fast exhaustion of the soluble hematin in the octanol phase.

To further grow these microcrystals, we used them as seeds for a second step of the crystallization procedure. We sonicated the two-phase solution and removed 50–100 μL of the citric buffer layer containing microcrystals. We prepared supersaturated solutions by dissolving commercial hematin powder in wet octanol at 70 °C. Because of the slow dissolution rate of amorphous hematin, this took approximately 3 weeks, during which the concentration of soluble hematin gradually increased. The hematin concentration in these solutions was determined by UV–vis spectrophotometry using an extinction coefficient of 3.1 ± 0.3 cm^{-1} mM^{-1} at a wavelength of 594 nm.[42] In all experiments, the final hematin concentration was between 0.1–0.4 mM, which exceeds the solubility of 0.07 mM at 25 °C.[42] We deposited the seeds suspended in citric buffer into 200 μL of this solution as illustrated in Figure 2C.

The citric buffer added to the wet octanol created a two-phase system. The seeds transferred to the octanol layer, likely

dx.doi.org/10.1021/cg5002682 | Cryst. Growth Des. 2014, 14, 2123–2127

owing to their hydrophobicity. This biphasic solution was incubated at 23 °C for up to 2−4 days. The two-phase solution was filtered through a 0.22 μm PVDT filter. The crystals held by the filter were rinsed with one milliliter of a 2% SDS solution in a 0.15 M $NaHCO_3$ or a 5% pyridine in water, to remove possible amorphous hematin, following published procedures.[19,45] Figure 3C demonstrates that within 1 h after their transfer to the hematin saturated two-phase solution, the seeds grow to about 5 μm. After 2−4 days, the crystals were about 30−35 μm, as seen in Figure 3D. This and other resulting crystals are well faceted and have smooth faces with no visible gaps. To identify the primary faces, we used the published values of the dihedral angles.[7] The crystal habit consists of $\{\bar{1}00\}$, {010}, and $\{0\bar{1}\bar{1}\}$ faces with ratios between their respective areas that are comparable to the hemozoin crystals found in *P. falciparum*.[7]

Longer growth times in the hematin saturated two-phase solution did not yield larger crystals. The limiting size could be due to exhaustion of the hematin in the solution or to accumulation of defects in the crystal; crystal defects lead to lattice strain that increases the free energy of the crystal, reduces the supersaturation, and facilitates growth cessation. To test the first scenario, we added freshly prepared hematin-saturated wet octanol to the top solution layer. Observation 2 weeks after the addition confirmed that this did not result in renewed growth, suggesting that the terminal crystal size is determined by the accumulation of defects in the crystals.

To understand the roles of the aqueous and organic phases for the nucleation and growth of large hematin crystals, we note that crystals grown in purely aqueous solutions are relatively small, around 2 μm in length, rounded and highly defective.[42] To test if crystals could be nucleated and grown in a single phase organic solution, we deposited about 20 mg of the amorphous commercial hematin in 2 mL of wet octanol. Within 2 days, well-faceted crystals of size 3−5 μm grew and had the habit illustrated in Figure 3D. Note that the same procedure performed in dry octanol did not yield any crystals.

With this, we conclude that the wet octanol layer of the two-phase system is the likely location where the crystals seen in Figure 3D grew. We propose that the role of the citric buffer phase is 2-fold: First, during nucleation, the citric buffer phase provides an aqueous/octanol interface. The ordering of the octanol molecules at this interface may serve as a suitable location for crystal nucleation, as suggested for the nucleation of hemozoin crystals in vivo.[21,25] Second, during growth, the citric buffer supplies hydrogen ions needed for the hydrogen bonds that link the hematin molecules in the crystal (see discussion of the hematin crystal structure above).

We tested several modifications to the procedure illustrated in in Figure 2. We stored the vials with seeded hematin-saturated wet octanol at 9, 23, 37, 45, 60, and 70 °C. The incubation temperature did not seem to affect the overall crystal size. If these vials were exposed to light, the crystal morphology was similar to the one of crystals grown in the dark; however, more distinctly faceted and larger crystal grew in vials stored in enclosures devoid of synthetic or natural light. Importantly, processes that employed either aqueous (pH 4.8) or anhydrous 1-octanol did not yield crystalline product at the nominal temperature and time of these studies. This confirmed the need to use a biomimetic two-phase system to mimic the lipid-aqueous environment of the parasites' digestive vacuole.

The procedure illustrated in Figure 2 is readily scalable if higher amounts of crystals are desired. During nucleation, the area of the interface between the organic and aqueous phase is an important parameter. Hence, a flat trough in which the citric buffer is deposited at the bottom and octanol at the top ensures a large surface area for the deposition of NaOH-dissolved hematin. The volume of added NaOH should scale with the volume of citric buffer at the bottom of the trough so that after homogenization of the NaOH concentration the pH remains below 5; higher pH values prevent crystallization by increasing hematin solubility.[23,42]

In summary, we have developed a biomimetic system that uses biphasic solutions to regulate nucleation and growth and to achieve crystal sizes inaccessible by conventional methods. To mimic the digestive vacuole of *P. falciparum*, we employ two-phase solutions, consisting of organic and aqueous layers. The method yields crystals with average dimensions of ca. 30 μm (and as long as 50 μm). In the biphasic system, the likely location of crystal growth is the organic phase, while the adjacent aqueous solution supplies hydrogen ions needed to bond hematin molecules in the crystal lattice. The organic/aqueous interface likely facilitates crystal nucleation by providing an ordered layer of octanol molecules. The availability of large hematin crystals opens new avenues for studies of hematin detoxification of malaria parasites and affords greater opportunity to use these materials for microscopic, spectroscopic, and crystallographic applications that are challenging for nanometer-size crystals.

AUTHOR INFORMATION

Corresponding Authors

*E-mail: vekilov@uh.edu.

*E-mail: jrimer@central.uh.edu.

Notes

The authors declare no competing financial interest.

ACKNOWLEDGMENTS

We thank Megan Ketchum for help with experimental procedures and for XRD characterization of hematin crystals, and David Sullivan for insightful discussion on hematin crystallization. This work was supported by NIH through the Nanobiology Interdisciplinary Graduate Training Program of the Gulf Coast Consortia for Quantitative Biomedical Sciences (Grant T32EB009379), NSF (Grant MCB-1244568), and The Welch Foundation (Grant E-1794).

REFERENCES

(1) Eastman, R. T.; Fidock, D. A. *Nat. Rev. Microbiol.* **2009**, *7*, 864−874.

(2) Bright, A. T.; Winzeler, E. A. *Nature* **2013**, *498*, 446−447.

(3) Sanchez, C. P.; Dave, A.; Stein, W. D.; Lanzer, M. *Int. J. Parasitol.* **2010**, *40*, 1109−18.

(4) Phyo, A. P.; Nkhoma, S.; Stepniewska, K.; Ashley, E. A.; Nair, S.; McGready, R.; ler Moo, C.; Al-Saai, S.; Dondorp, A. M.; Lwin, K. M.; Singhasivanon, P.; Day, N. P. J.; White, N. J.; Anderson, T. J. C.; Nosten, F. *Lancet* **2012**, *379*, 1960−1966.

(5) Brown, W. H. *J. Exp. Med.* **1911**, *13*, 290−299.

(6) Buller, R.; Peterson, M. L.; Almarsson, O.; Leiserowitz, L. *Cryst. Growth Des.* **2002**, *2*, 553−562.

(7) Weissbuch, I.; Leiserowitz, L. *Chem. Rev.* **2008**, *108*, 4899−4914.

(8) Bannister, L. H.; Hopkins, J. M.; Fowler, R. E.; Krishna, S.; Mitchell, G. H. *Parasitol. Today* **2000**, *16*, 427−433.

(9) Nagaraj, V. A.; Sundaram, B.; Varadarajan, N. M.; Subramani, P. A.; Kalappa, D. M.; Ghosh, S. K.; Padmanaban, G. *PLoS Pathogens* **2013**, DOI: 10.1371/journal.ppat.1003522.

(10) Ursos, L. M. B.; DuBay, K. F.; Roepe, P. D. *Mol. Biochem. Parasitol.* **2001**, *112*, 11−17.
(11) Noland, G. S.; Briones, N.; Sullivan, D. J. *Mol. Biochem. Parasitol.* **2003**, *130*, 91−99.
(12) Pagola, S.; Stephens, P. W.; Bohle, D. S.; Kosar, A. D.; Madsen, S. K. *Nature* **2000**, *404*, 307−310.
(13) Slater, A. F. G.; Swiggard, W. J.; Orton, B. R.; Flitter, W. D.; Goldberg, D. E.; Cerami, A.; Henderson, G. B. *Proc. Natl. Acad. Sci. U. S. A.* **1991**, *88*, 325−329.
(14) Bohle, D. S.; Dinnebier, R. E.; Madsen, S. K.; Stephens, P. W. *J. Biol. Chem.* **1997**, *272*, 713−716.
(15) Oliveira, M. F.; Kycia, S. W.; Gomez, A.; Kosar, A. J.; Bohle, D. S.; Hempelmann, E.; Menezes, D.; Vannier-Santos, M. A.; Oliveira, P. L.; Ferreira, S. T. *FEBS Lett.* **2005**, *579*, 6010−6.
(16) Gligorijevic, B.; Bennett, T.; McAllister, R.; Urbach, J. S.; Roepe, P. D. *Biochemistry* **2006**, *45*, 12411−12423.
(17) Hayward, R.; Saliba, K. J.; Kirk, K. *J. Cell Sci.* **2006**, *119*, 1016−1025.
(18) Coppens, I.; Vielemeyer, O. *Int. J. Parasitol.* **2005**, *35*, 597−615.
(19) Ambele, M. A.; Sewell, B. T.; Cummings, F. R.; Smith, P. J.; Egan, T. J. *Cryst. Growth Des.* **2013**, *13*, 4442−4452.
(20) Hoang, A. N.; Ncokazi, K. K.; de Villiers, K. A.; Wright, D. W.; Egan, T. J. *Dalton Trans* **2010**, *39*, 1235−44.
(21) Kapishnikov, S.; Weiner, A.; Shimoni, E.; Guttmann, P.; Schneider, G.; Dahan-Pasternak, N.; Dzikowski, R.; Leiserowitz, L.; Elbaum, M. *Proc. Natl. Acad. Sci. U. S. A.* **2012**, *109*, 11188−11193.
(22) Egan, T. J.; Mavuso, W. W.; Ncokazi, K. K. *Biochemistry* **2001**, *40*, 204−13.
(23) Egan, T. J.; Chen, J. Y. J.; de Villiers, K. A.; Mabotha, T. E.; Naidoo, K. J.; Ncokazi, K. K.; Langford, S. J.; McNaughton, D.; Pandiancherri, S.; Wood, B. R. *FEBS Lett.* **2006**, *580*, 5105−5110.
(24) Pisciotta, J. M.; Coppens, I.; Tripathi, A. K.; Scholl, P. F.; Shuman, J.; Bajad, S.; Shulaev, V.; Sullivan, D. J. *Biochem. J.* **2007**, *402*, 197−204.
(25) Kapishnikov, S.; Berthing, T.; Hviid, L.; Dierolf, M.; Menzel, A.; Pfeiffer, F.; Als-Nielsen, J.; Leiserowitz, L. *Proc. Natl. Acad. Sci. U. S. A.* **2012**, *109*, 11184−11187.
(26) Egan, T. J.; Ross, D. C.; Adams, P. A. *FEBS Lett.* **1994**, *352*, 54−57.
(27) Egan, T. J. *Mol. Biochem. Parasitol.* **2008**, *157*, 127−136.
(28) de Villiers, K. A.; Egan, T. J. *Molecules* **2009**, *14*, 2868−87.
(29) Soares, J.; Menezes, D.; Vannier-Santos, M. A.; Ferreira-Pereira, A.; Almeida, G. T.; Venancio, T. M.; Verjovski-Almeida, S.; Zishiri, V. K.; Kuter, D.; Hunter, R.; Egan, T. J.; Oliveira, M. F. *PLoS Neglect. Trop. Dis.* **2009**, DOI: 10.1371/journal.pntd.0000477.
(30) Sullivan, D. J. *Int. J. Parasitol* **2002**, *32*, 1645−1653.
(31) Kappe, S. H. I.; Vaughan, A. M.; Boddey, J. A.; Cowman, A. F. *Science* **2010**, *328*, 862−866.
(32) Solomonov, I.; Osipova, M.; Feldman, Y.; Baehtz, C.; Kjaer, K.; Robinson, I. K.; Webster, G. T.; McNaughton, D.; Wood, B. R.; Weissbuch, I.; Leiserowitz, L. *J. Am. Chem. Soc.* **2007**, *129*, 2615−2627.
(33) Straasø, T.; Kapishnikov, S.; Kato, K.; Takata, M.; Als-Nielsen, J.; Leiserowitz, L. *Cryst. Growth Des.* **2011**, *11*, 3342−3350.
(34) Moody, A. *Clin. Microbiol. Rev.* **2002**, *15*, 66−78.
(35) Bell, D.; Wongsrichanalai, C.; Barnwell, J. W. *Nat. Rev. Microbiol.* **2006**, *4*, 682−695.
(36) Wilson, M. L. *Clin. Infect. Dis.* **2012**, *54*, 1637−1641.
(37) Kurosawa, Y.; Dorn, A.; Kitsuji-Shirane, M.; Shimada, H.; Satoh, T.; Matile, H.; Hofheinz, W.; Masciadri, R.; Kansy, M.; Ridley, R. G. *Antimicrob. Agents Chemother.* **2000**, *44*, 2638−2644.
(38) de Villiers, K. A.; Kaschula, C. H.; Egan, T. J.; Marques, H. M. *J. Biol. Inorg. Chem.* **2007**, *12*, 101−117.
(39) Asher, C.; de Villiers, K. A.; Egan, T. J. *Inorg. Chem.* **2009**, *48*, 7994−8003.
(40) Gildenhuys, J.; Roex, T. l.; Egan, T. J.; de Villiers, K. A. *J. Am. Chem. Soc.* **2012**, *135*, 1037−1047.
(41) Dill, K.; Bromberg, S. *Molecular Driving Forces: Statistical Thermodynamics in Chemistry and Biology*; Garland Science: New York, 2003.
(42) Ketchum, M. A.; Olafson, K. N.; Petrova, E. V.; Rimer, J. D.; Vekilov, P. G. *J. Chem. Phys.* **2013**, *139*, 121911.
(43) Wick, C. D.; Chang, T.-M. *J. Phys. Chem. B* **2014**. DOI: 10.1021/jp411427a.
(44) Brown, S. B.; Jones, P.; Suggett, A. *Trans. Faraday Soc.* **1968**, *64*, 986−993.
(45) Ambele, M. A.; Egan, T. J. *Malar J.* **2012**, *11*, 337−350.
(46) Chong, C. R.; Sullivan, D. J., Jr. *Biochem. Pharmacol.* **2003**, *66*, 2201−2212.